Fast fully automatic stroke lesions segmentation based on Parzen estimation and μ-law in skull CT images.

Lucas de O. Santos [*] **Aldísio G. Medeiros** [**]
Pedro P. Rebouças Filho [***]

[*] *Instituto Federal de Educação, Ciência e Tecnologia do Ceará - IFCE, CE (e-mail: lucas.santos@lapisco.ifce.edu.br)*
[**] *Universidade Federal do Ceará - UFC, CE (e-mail: aldisio.medeiros@lapisco.ifce.edu.br)*
[***] *LAPISCO-Laboratório De Processamento de Imagem,Sinais e Computação Aplicada (e-mail: pedrosarf@ifce.edu.br)*

Abstract: Stroke is the second leading cause of death worldwide. Those who survive usually experience vision loss, speech, paralysis, or confusion. Agile diagnosis proves to be decisive for patient survival. This paper presents a proposal for rapid stroke segmentation in cranial CT scans, with 1 second, on average, by sample. The segmentation stage uses Parzen window density estimation to classify potentially injured regions in this approach. A proposed adaptation of the μ-law algorithm is applied to enhance damaged areas about healthy brain regions. The results show that the proposed method has the highest mean of accuracy, reaching 99.85%, with a specificity of 99.94%, surpassing classical methods by 16%. On the other hand, the algorithm presented similarity indexes of 93.39% for the Matthews correlation coefficient and DICE of 93.35%. The proposed methodology also compared the results with four approaches that use deep learning; it proved to be equivalent in accuracy, DICE, and specificity, with superior results in sensitivity up to 8% to one of the approaches based on the recent Detectron2 neural network. The results indicate that the proposed method is competitive concerning the approaches already presented in the literature.

Keywords: Stroke region segmentation, Parzen window, level set, μ-law, aid to medical diagnosis.

1. INTRODUCTION

Stroke is the leading cause of disability in the world. It is estimated that 70% of patients who have suffered a stroke do not return to work due to sequelae or because they need specific care. The most significant consequences are difficulties in speech, motor coordination, locomotion, and cognitive delays. The degree of disability is directly related to the fastness of diagnosis and appropriate treatment. The longer the time of diagnosis, the greater the chances of aftereffects of the disease that cause disability. Oesch et al. (2021). Therefore, detecting the lesion contributes to a fast diagnosis that improves patient survival Virani et al. (2020); Han et al. (2020).

The lesion is characterized by the drastic reduction in the supply of nutrients and oxygen through the blood system to a particular brain region. This condition commonly represents characteristics of ischemic stroke, when there is an obstruction or abrupt reduction of blood flow. On the other hand, when blood vessels rupture, causing cerebral hemorrhage is characterized as a hemorrhagic stroke. In both cases, rapid diagnosis is one of the most critical stages in therapy to establish the course of treatment, recognizing the type and location of the lesion Oesch et al. (2021).

The computed tomography (CT) exams of the skull are one of the most used techniques for the rapid diagnosis of the patient because this technique presents a lower cost, more quickness, and is a non-invasive procedure. In this scenario, image analysis stands out in the clinical evaluation, helping the specialist identify the lesion region, assess the size of the affected brain area, and thus establish the diagnosis and preliminary treatment of the pathology Medeiros et al. (2020); Han et al. (2020).

Several studies have directed efforts towards developing algorithms that automatically detect lesions through CT exams in recent years. This stage is critical to classifying the type of stroke to define the medical procedure in the preliminary treatment. Yahiaoui et al. Yahiaoui and Bessaid (2016) a multiscale contrast enhancement combined with Laplacian Pyramid (LP) is proposed to enhance the lesion region to identify the stroke region of interest (ROI). Karthik et al. Karthik and Menaka (2017) suggest using curvelet transformation to identify attributes and include a classification stage with SVM classifier. On the other hand, Sivakumar et al. Sivakumar and Ganeshkumar (2017) developed a heuristic-based histogram equalization, combining feature extraction with the Adaptive Fuzzy Inference classifier.

Other recent approaches present the application of techniques based on deep learning. Zhang et al. Zhang et al. (2018) suggests an automated process to detecting and segmenting ischemic stroke lesions using fully convolutional DenseNets. The work by Han et al. Han et al. (2020) features a stroke detection combining deep features extracted from Extreme Inception, Inception V3, VGG architectures and combines with the SVM with the Radial Basis Function (RBF) Kernel classifier. The approaches based on deep learning present promising results; however, commonly, these solutions present limitations for applications with low computational resources.

This work proposes a new probabilistic approach based on Parzen density estimation for classifying regions to detect hemorrhagic stroke on CT images of the skull. Fully automatic segmentation combined an adaptation of the μ-law algorithm to highlight the lesion candidate region as a previous step to probabilistic classify the pixels. This approach evaluates radiological densities of the skull to establish a safe area for the study of the lesion. Our method is called Level Set Based on Radiological Densities inspired by the μ-Law (LSBRD-μ), as an evolution of the traditional Level Set algorithm originally proposed by Osher and Sethian Osher and Sethian (1988).

The results of the proposed method are compared with recent approaches in the literature, LSCPM Rebouças et al. (2017), Fuzzy C-means (FCM), Ada-MGAC Medeiros et al. (2020), and the recent method known as FPLS de Souza Rebouças et al. (2021). In addition, the proposed evaluation compares the results against classic techniques as Watershed Körbes and Lotufo (2010) and Region Growing Rouhi et al. (2015), besides different deep learning-based methods. Specifically, this article offers the following study and contributions:

(1) A fully automatic approach to hemorrhagic stroke segmentation;
(2) Classification based on probability density as a low computational cost technique;
(3) Image enhancement based inspired by μ-Law;
(4) Low detection time.

This work is organized as follows: Section 2 presents the segmentation techniques evaluated in this study, and the section 3.1 the main techniques used as the theoretical basis of this study. The section 4 presents the proposed methodology and in Section 5 the results are discussed based on the evaluation metrics. Finally, the section 6 presents contributions, conclusions and proposals for future studies.

2. RELATED WORKS

The main works related to the study of identification and segmentation of strokes based on segmentation of computed tomography images are presented in this section. The main theoretical foundations that inspire this work are detailed at the end of this section.

2.1 Classical approaches

Watershed-transform and Region Growing On the other hand, the Watershed algorithm has been widely evaluated in the literature, highlighting its recent application in stroke detection in work by Körbes and Lotufo Körbes and Lotufo (2010), in addition to the studies by Benson et al. Benson et al. (2015) applied to identify brain lesions on magnetic resonance imaging.

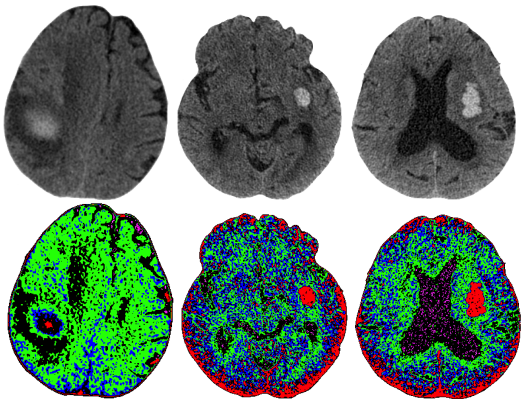

Figure 1. From left to right, three examples of the analysis of cerebral radiological densities. The first line shows the CT scan image, in the second line shows different densities of intracranial tissue. This is an analysis of the HU densities of the skull (spinal fluid in magenta, white mass in green, gray matter in blue, blood in red). The lesion is highlighted in red inside the skull.

As a classic technique, the Watershed algorithm depends directly on the intensity variations in the image, so it is sensitive to contrast oscillations. However, computed tomography images present different contrast variations.

Fuzzy C-means clustering The Fuzzy C-means (FCM) method presents a behavior based on the similarity between pixels in a region, proposed by Dunn Dunn (1973). Pixels are grouped according to their characteristics through iterative minimization of the cost function J, defined in Equation 1. The similarity is calculated according to the Euclidean distance of the pixels, with a central pixel representing the region's characteristics defined by the already grouped pixels. This segmentation aims to partition the image into areas with significant features according to the similarity criterion. The cost function J is defined by

$$J = \sum_{i=1}^{N} \sum_{j=1}^{D} u_{ij}^{m} \ \|z_i - c_j\|^2 , \tag{1}$$

Where N is the number of pixels to be evaluated, z_i represents the evaluated pixel, c_j indicates the reference pixel of the partition, u_{ij} defines the similarity and m is the fuzzy parameter.

FCM shows promising results in low-contrast imaging, such as CT of the brain. However, this algorithm uses Euclidean distance as a similarity metric between each pixel evaluated about the formed clusters. This procedure is computationally expensive for time-constrained applications.

Level Set Based on Analysis of Brain Radiological Densities Rebouças et al. Rebouças et al. (2017) proposed the Level Set based on analysis of radiological densities. It is inspired by the segmentation algorithm known as Level

Set, initially proposed by Sethian (1999b). An evaluation of the stroke region is presented based on the density of the tissue represented in the image under Hounsfield (UH) Units, adopting 80UH for window width and 40 UH for center level. Figure 1 presents an example of tissue analysis from densities.

Rebouças et al. method initializes from on a circle centered in a region previously defined based on the intensity of the pixels. However, stroke lesions do not have a regular shape, making it challenging to correctly represent the region in simple geometric shapes. This characteristic can lead the method to fail when external areas to the lesion have similar intensities.

Geodesic Active Contour Method Medeiros et al. Medeiros et al. (2020) presented a method called Ada-MGAC inspired by techniques from mathematical morphology. According to the Level Set approach, proposed by Sethian (1999b), Ada-MGAC presents the detection of stroke as a geodesic active contours model does not depend on the parameterization of the curve. The detection of the curve that defines the region corresponds to the geodesics of a riemannian space whose metric can be defined by $g(I)$. This energy minimization can be represent by:

$$C(C) = \int_0^{length(C)} g(I)(C(s))ds \tag{2}$$

Although it presents a fast convergence process, Ada-MGAC method does not offer any pixel classification stage, depending only on the similarity of the intensity of the nearby pixels, which can lead to detections of regions that go beyond the lesion region.

2.2 Recent approaches based on Deep Learning

Detectron2 network with fine tuning Recent works use Convolutional Neural Networks (CNN) as feature extractors, known as deep feature extractors. In this sense, it uses the output of neurons from the last convolutional layer as a sample feature vector. In work by Han et al. Han et al. (2020) the identification of stroke is proposed in two stages. The first stage combines the Extreme Inception, Inception V3, VGG CNNs as feature extractors with the SVM with the Radial Basis Function (RBF) Kernel classifier. This stage sorts the pixels and identifies if there is an initial region of interest. The second stage combines the output of the first stage with the Detectron2 deep neural network, proposed by Facebook Artificial Intelligence Research (FAIR), to identify the lesion region. Detectron2 network is combined with Parzen window (Detectron2-fλ), K-means clustering (Detectron2-fδ), and with Region Growth (Detectron-f).

The work of Han et al. Han et al. (2020) shows promising high rates of accuracy and sensitivity in the detection of stroke. However, two stages of model training and classification were necessary to achieve better results. In addition, the authors presented the need for specific hardware such as a GPU card that can compromise its use in low-cost applications.

The methodology proposed in this work evaluates all algorithms, considering the result of the method's segmentation about the specialist manual segmentation. The following sections present the results and assess the method proposed in this work.

3. MATERIALS AND METHODS

3.1 Materials and Methods

In this Section we present the techniques that inspired the construction of the proposed approach. Subsection 3.2 describes the theoretical foundation of the Level Set segmentation algorithm. A description of Probabilistic classification based on the Parzen is described in Subsection 3.3. Subsection 3.4 presents the μ-law Algorithm, and Subsections 3.5 the dataset used in the experiments. Finally, we present the evaluation metrics in subsection 3.6 proposed in this work.

3.2 Level set

Within the context of segmenting regions into images, Osher and Sethian Osher and Sethian (1988) proposed a numerical solution based on implicit contours called Level Set, where the originally parametric segmentation curve is represented under the surface, transforming the problem into a geometric model.

Let a two-dimensional space with two regions and that there is a boundary between them. Assume $C(x, y)$ as a function that defines the boundary. The idea of the implicit contour is to represent C in a function ϕ that can deform the boundary, thus defining new positions for the points. For this, we add a third component to space that represents time. We call the new boundary function $\phi[(x, y), t]$. Making the function $\phi[(x, y), t = 0] = C(x, y)$, we have an initial value for the function ϕ. We, therefore, have, for $\phi[(x, y), t = 0]$ the Level Set zero.

The curve $C(x, y)$ becomes a level curve embedded in the Level Set ϕ. This can be done, for example, using a signed distance function. Equation 3 presents this description:

$$\phi[(x, y), t] = \begin{cases} -sign(x, y, C) & \text{, if (x,y) is out of C curve} \\ sign(x, y, C) & \text{, otherwise.} \end{cases} \tag{3}$$

where *sign* denotes the distance from the point (x, y) to the closest point on C. In this representation, one of the advantages is that we do not consider the parameterization of the curve itself, but the region circumscribed by the curve. By manipulating ϕ which defines a new boundary for the C curve. This modeling also offers adaptation to topological changes, as illustrated in Figure 2.

The design of the level set theory proposed by Sethian (1999a) is based on the Hamilton-Jacobi equation. This theory states that a closed curve $\boldsymbol{\phi} : R^2 \times R^+ \rightarrow R$ evolves due to a velocity field $\pm F\boldsymbol{\eta}$, where $(\pm\boldsymbol{\eta})$ is the unit vector that is perpendicular to $\boldsymbol{\phi}$, as shown in Figure 3.

The Level set zero is the initial state of the surface (or defined level function) and consists of an image with the same dimensions as the image to be segmented. Level set zero, illustrated in Figure 3, can be formed by a single binary component or multiples disconnected ones, which can join or split during the evolution of the segmentation curve to delimit the region of interest.

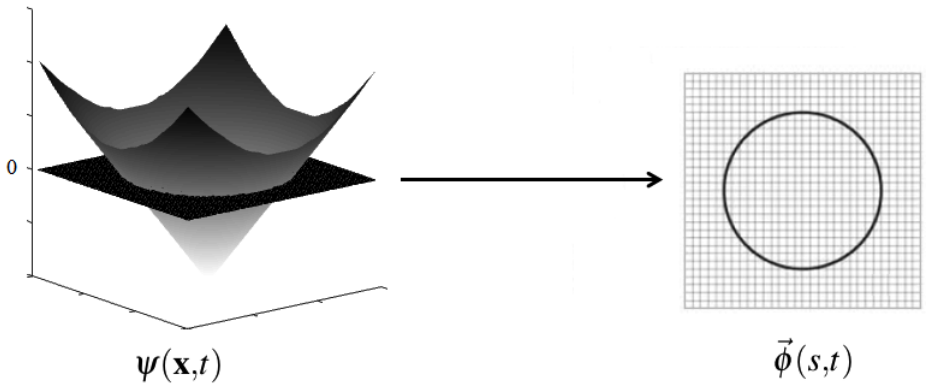

Figure 2. Level set function representation $\psi(\mathbf{x}, t)$ and the curve $\boldsymbol{\phi}(s, t)$. Adapted from Sethian (1999a).

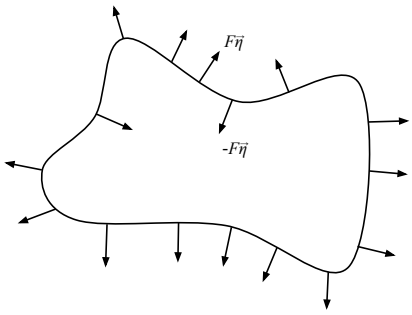

Figure 3. Propagation of a closed curve $\boldsymbol{\phi}$ subjected to a velocity field ($\pm F\boldsymbol{\eta}$). Adapted from Reboucas et al. (2016).

3.3 Parzen window

The Parzen Window Theodoridis and Koutroumbas (2009) is a non-parametric type of probability density estimation method. This algorithm does not assume a probability distribution of the data. This approach calculates the probability that a point z belongs to a non-Euclidean region defined by a hypercube $R = \{\mathrm{z_i}\}_{\mathrm{i=1}}^{\mathrm{k}}$ with dimensionality d as in the X Equation 4:

$$p(z) = \frac{1}{k} \sum_{i=1}^{k} \varphi \left(\frac{z_i - z}{h} \right), \tag{4}$$

where φ is the kernel function used to limit the neighborhood, h is the hypercube edge size and k is the number of pixels of R.

The Gaussian kernel is the most used function in the literature to evaluate the probability from the neighborhood of points because it has relevant properties. The first property is that the Gaussian function has a smoothed surface, which contributes to the fact that the density estimation function $p(z)$ also presents a smooth variation. Another property is that the family of Gaussian functions can be represented in a radially symmetrical perspective. In this way, the function can be declared in detail identified only by a variance. In this sense, the function $p(z)$ can be defined as a combination of radially symmetric Gaussian kernels Yeung and Chow (2002).

The Gaussian kernel used in this work has the same characteristics described according to Bishop (2006) and presented in Equation 5:

$$\varphi(z_i, z) = \frac{1}{\sqrt{(2\pi)^d |\Lambda|}} \exp\left(-\frac{(z_i - z)^{\Lambda - 1}(z_i - z)}{2} \right), \tag{5}$$

where z and z_i are feature vectors $\in R^d$ Λ is the covariance matrix $\in R^{d \times d}$ and $|\Lambda|$ is the determinant of Λ.

3.4 μ-law Algorithm

According to Ribeiro Ribeiro (2017), The μ Law algorithm (μ-law), also approximated by the μ Law, is a compression and expansion algorithm used mainly in Code Modulation telecommunications systems 8-bit Pulse (Faruque, Saleh Faruque (2015)) in North America and Japan. This algorithm is one of two algorithms presented in the ITU-T (International Telecommunication Union Telecommunication Standardization Sector) G.711 standard. Compression and expansion algorithms, represented by the term companding, aim to reduce a channel's noise and distortion effects with a limited dynamic range. In analog systems, it is possible to obtain an increase in the Signal Rapid Ratio (SNR). In contrast, in digital systems, it is possible to get a reduction in the quantization error. The compression algorithm is used by the signal transmitter. Given an input signal" x," the compression algorithm of the Law μ can be described in analog form according to the Equation 6:

$$F(x) = sgn(x) \cdot \frac{ln(1 + \mu \cdot |x|)}{ln(1 + \mu)}, \tag{6}$$

where $sgn(x)$ is a function that indicates the sign of the input value x and μ=255 for 8-bit applications (North American and Japanese standard).

In the context of digital image signals, the compression equation lei-μ can express be according to the Equation 7.

$$M(x, y) = f(x, y) \cdot \frac{ln[1 + \mu \cdot f(x, y)]}{ln(1 + \mu)} \tag{7}$$

3.5 Datasets

CT images were obtained with the support of the Trajano Almeida (Diagnostic Imaging) clinic and used in previous studies (Rebouças et al. Rebouças et al. (2017), Rebouças et al. (2017)). Patient-sensitive data bein omitted in all analyses of this study.

3.6 Evaluation Metrics

Seven evaluation metrics were used to verify the classifiers performance: Accuracy (ACC), Sensitivity (TPR),

Specificity (SPC), Precision (PPV), Matthews correlation coefficient (MCC), Dice (DSC) and Jaccard (JSC). The calculation is done through the confusion matrix generated by the classifiers, according to True Positive (TP), False Negative (FN), False Positive (FP), and True Negative (TN) Hossin and Sulaiman (2015).

4. APPROACH BASED ON PARZEN ESTIMATION AND μ-LAW FOR STROKE SEGMENTATION IN SKULL CT IMAGES

4.1 Step 1: Skull segmentation process

A threshold applied to segment the skull region was in the specific range for bones, which is 200 HU. In this way, all pixels above this threshold characterize the brain bone or other noises coming from the machine where was performed a CT scan. The result of this process can be seen in Figure 6 in items a), b), and c) of Step 1. After that, a mathematical operation of intersection between the two images of things a) and b) of the exact figure is performed to obtain only the patient's brain region, item c).

After removing the patient's skull, was applied a blurring filter to smooth the image contours, item d) of Step 1 of Figure 6. That's done so that small area noises are reduced.

4.2 Step 2: Preprocessing with μ-law and Region of interest detection

The pixel range that contains the bleeding regions is between 56 to 76 HU, Rebouças et al. Reboucas et al. (2019). However, using only a thresholding function in the grayscale image to separate the area of interest from the image produces a lot of noise around the lesion. That is because different brain regions can have the same pixel intensity. In this sense, only a thresholding function is not practical enough to locate the bleeding part.

However, if this pixel range is reducing, some information about both noise and the lesion is also reduced. Thus, the threshold used in this work is more restrictive and, therefore, with a smaller range than the standard. Although a small part of the lesion has been reduced, the stroke is still pre-segmented in all cases.

Given character, the μ-Law, when applied in a region, the pixels' intensities in that location tend to get closer. That causes a level of lightning in the image. In this way, the μ-law has applied to the range of pixels that do not match the Avg. That range has where reduced, as seen earlier. Therefore, the region undergoes a lightening in pixels, as can be seen in Figure 4 in items a) and b). Thus, there was a considerable difference between pixels that are lesion and those that are not. Figure 5 shows a comparison between the use of the μ-law for noise removal and thresholding using the complete threshold of the hemorrhagic region.

Although there is a considerable gain in reducing noisy image elements, a post-processing step is necessary so that only one part serves as input for the classification. In this sense, a morphological erosion operation was applied to the image before applying a threshold. That was necessary to circumvent the effects resulting from the limitation of the pixel intensity range that characterizes hemorrhagic stroke

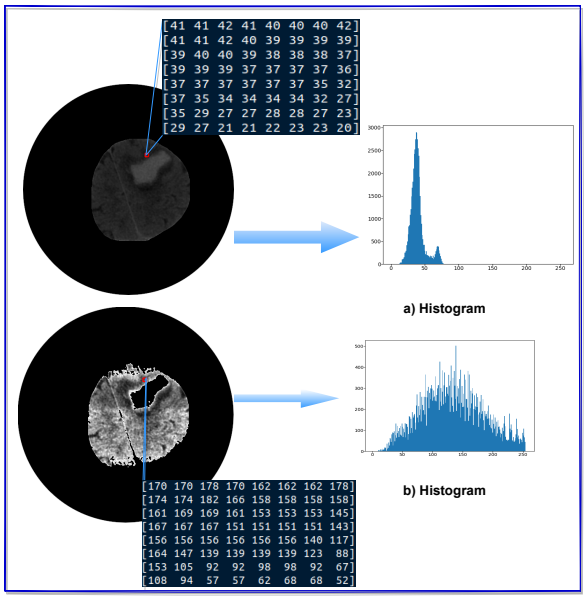

Figure 4. Histogram comparison. a) Histogram of the original image; b) Histogram of the image after the application of the μ-law

(HS), as described in 4.2, which caused a slight loss of lesion information, as can be seen in Step 2 of Figure 6, in the law enforcement image μ. The effects can be observed in item a), where the internal region of the lesion presents less noise than in the previous step. After this process, a morphological dilation operation is applied to filter out the most significant noise in terms of the area still present in the image, especially at the edges, item b). After this step, to highlight the lesion area a little more, and was performed an erosion operation, item c). Finally, the most significant component in terms of size is the filter from the image (item d), which is the initialization Level Set used in 4.3.

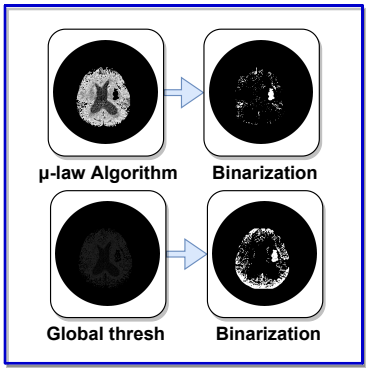

Figure 5. Noise level comparison bein based on applying the μ-law and thresholding in the intensities of normal HS pixels in the same image.

4.3 Step 3: Level Set Initialization

As the lesion region is located, 4.2, it is used as the initialization Level Set of the Parzen Window. Parzen windowing classifies the pixels that are or are not part of the lesion. Figure 6 in Step 3 shows the visual results of the evolution of the Level Set curvature. Tables 2, 1 and 4

show the average results of the qualitative and quantitative metrics applied in the validation process of the generated results. The active contour iterates over each pixel in the image. Thus, the larger the picture, the longer the estimated time for processing to finish. In this sense, before Parzen bein applied to the impression, it is reduced by 50% of its original size, and at the end method, it increases the original size. This process proved to be effective both in evaluative metrics and in the average processing time per image.

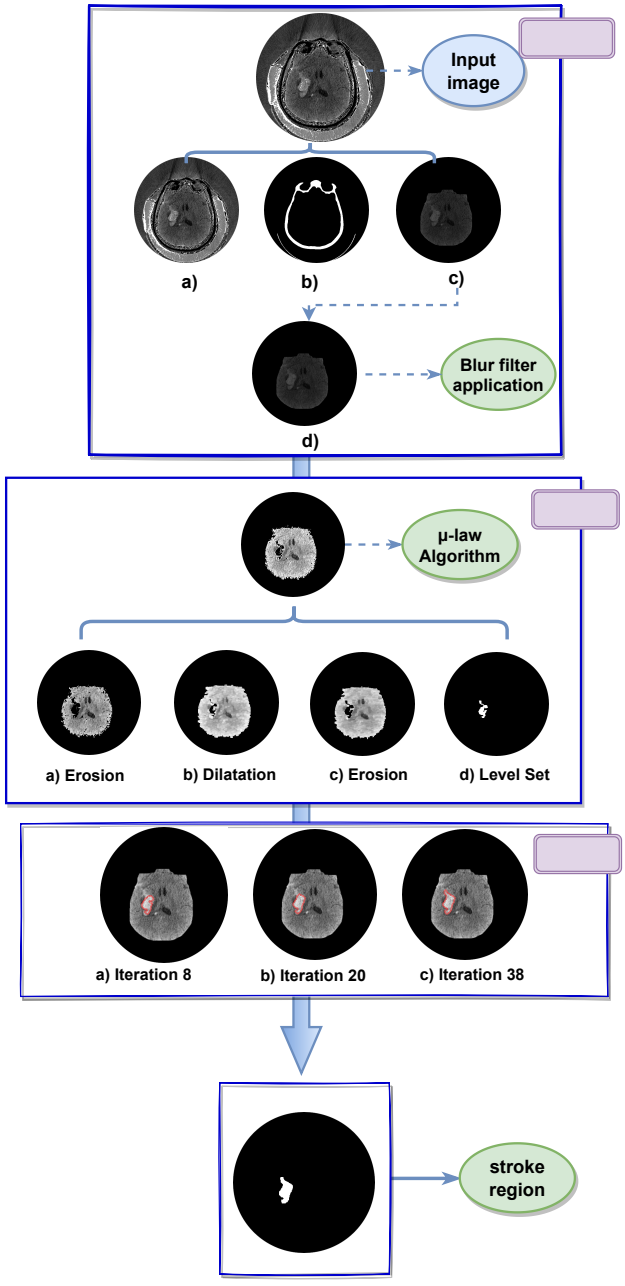

Figure 6. Flowchart of the method applied.

5. RESULTS AND DISCUSSION

In this section, the results obtained by the LSBRD-μ are present. To validate the results obtained, the database described in 3.5 bein used.

Table 1 shows the results of the MCC, DSC, and JSC metrics and also their respective standard deviations. As can be seen, for the MCC metric, the LSBRD-μ is superior by 2.04% the methods Medeiros et al. Medeiros et al. (2020), which is the one with the best score (91.35%), respectively. Furthermore, the method Korbe et al. Körbes and Lotufo (2010) presents the worst indexes for this metric with 86.87%, being surpassed by the LSBRD-μ in 6.52%. Considering the DSC metric, the proposed method obtained the best values, being more effective than the Medeiros et al. Medeiros et al. (2020) method by 2.07%. As the Medeiros et al. Medeiros et al. (2020) method is the most effective among the competitors with a 91.28% hit rate, it is was understood that the LSBRD-μ is more accurate than the others. For the JSC metric, was repeated the same comparative logic, as the Medeiros et al. Medeiros et al. (2020) method is the best among the competitors. However, the proposed method is the most effective, as it outperforms the Medeiros et al. Medeiros et al. (2020) method by 3.45% and the Korbe et al. Körbes and Lotufo (2010) method by 10.49%, which obtained the lowest performance for this metric.

These MCC, DSC, and JSC metrics express the level of proximity between the segmented image and the one marked by the specialist. Thus, it is was understood that the LSBRD-μ is closer to the gold standard of segmentation than the others. Furthermore, the standard deviation values obtained are the smallest, being 1.18% lower than the Medeiros et al. Medeiros et al. (2020) methods for the MCC metric. Considering the DSC metric, the LSBRD-μ is 1.25% lower than the Medeiros et al. Medeiros et al. (2020) method and 6.72% lower than the Korbe et al. Körbes and Lotufo (2010) method, which is the worst among all. The same logic extends to JSC metrics, where the proposed method is 1.85% lower than the Medeiros et al. Medeiros et al. (2020) method, which is the best among the others. These data allow us to state that the dataset processed by the LSBRD-μ presents a low fluctuation of values, and this gives the method a smaller data dispersion.

Table 1. Results from the Matthews Correlation Coefficient (MCC), DICE Similarity Coefficient (DSC) and Jaccard Similarity Coefficient (JSC) with their respective standard deviations.

Algorithm	Year	MCC(%)	DSC(%)	JSC(%)
LSBRD-μ	2022	**93.39 ± 02.68**	**93.35 ± 02.80**	**87.66 ± 04.77**
Medeiros et al.Medeiros et al. (2020)	2020	91.35 ± 03.86	91.28 ± 04.05	84.21 ± 06.62
Rebouças et al. Rebouças et al. (2017)	2017	89.27 ± 05.78	88.85 ± 06.51	80.50 ± 09.79
Rouhi et al.Rouhi et al. (2015)	2015	80.58 ± 16.90	79.26 ± 18.30	68.23 ± 17.20
Korbe et al. Körbes and Lotufo (2010)	2010	86.87 ± 07.41	86.63 ± 07.84	77.17 ± 11.20
Dunn Dunn (1973)	1973	88.00 ± 16.80	87.41 ± 18.50	80.77 ± 19.20

Table 2 shows the results of PPV, TRP, and SPC and also their respective standard deviations. As can be seen, the proposed method presents the highest indexes in the SPC metric, being 16.91% higher than the Rebouças et al. Rebouças et al. (2017) method, which is the worst among all. Furthermore, even though the value is equal to that obtained in Medeiros et al.Medeiros et al. (2020), the proposed way is more concise when analyzed from the standard deviation point of view. In the context of this work, the SPC metric indicates how effective the method is in asserting that a given region is not an HCV. The proposed algorithm is the most effective from this

point of view. Although the technique does not have the best indices in the PPV and TPR metrics, it proves to be competitive to the others, being even superior to the Medeiros et al.Medeiros et al. (2020) method in the TPR metric, surpassing it by 10.01%, being this method more current in the literature when compared to others.

Table 2. Results of precision (PPV), sensitivity (TPR), and specificity (SPC) with their respective standard deviations.

Algorithm	Year	PPV(%)	TPR(%)	SPC(%)
LSBRD-μ	2022	**93.78 ± 05.75**	**93.35 ± 04.23**	**99.94 ± 00.05**
Medeiros et al.Medeiros et al. (2020)	2020	99.88 ± 00.09	93.46 ± 04.32	99.93 ± 00.05
Rebouças et al.Rebouças et al. (2017)	2017	99.75 ± 00.25	99.96 ± 00.05	83.03 ± 11.13
Rouhi et al.Rouhi et al. (2015)	2015	99.00 ± 04.36	99.66 ± 00.23	92.84 ± 21.88
Korbe et al.Körbes and Lotufo (2010)	2010	99.84 ± 00.19	99.85 ± 00.11	87.32 ± 13.38
Dunn Dunn (1973)	1973	99.32 ± 02.99	99.86 ± 00.10	90.53 ± 21.31

Another relevant analysis is the method's performance in terms of the time required to segment the lesion in the images. The importance of this analysis is related to care by physicians given to patients diagnosed with stroke. The faster the method, the quicker and more accurate the diagnosis and treatment of this disease. In this sense, when looking at the 4 Table, it is noted that the proposed method has an average segmentation time of only 1.14 seconds. This value is smaller than the one obtained by the Medeiros et al.Medeiros et al. (2020) method, which has an average time of 1.50 seconds. Thus, the proposed method is the fastest among all and presents a low value of standard deviation, implying a low dispersion of the data.

The methods compared above do not use algorithms based on deep learning networks. However, Table 3 shows the results that the Detectron 2 algorithm obtained for the same database used in this work. In this sense, the proposed method presents competitive results with those of the Detectron 2 network, being even higher by 0.56% in the sensitivity metric. That shows that LSBR-μ can predict if the detected region bein corrupted with Avg. For the Dice metric, the method is superior to Detectron-$\boldsymbol{f\lambda}$ by 1.98%. This logic extends to accuracy, with the proposed method superior to this same network by 0.02%.

Regarding segmentation time, Table 4 shows that the proposed method is the second-fastest in lesion segmentation. It is worth mentioning that the segmentation time of methods based on deep learning does not take into account what was spent in the training stage so that the network could perform the stroke detection process on these images.

The use of deep learning is not always feasible because it requires a high computational power to perform the network training steps. That is possible with the help of GPU to accelerate the algorithm training process. In addition, the training process needs lesioned images segmented by the specialist. Therefore, the effectiveness proposed by these algorithms bein proportionally linked to the number of images used in the training steps.

However, the proposed method executes using simple CPU hardware to process the data and does not need images for large training. That shows that LSBRD-μ is easy to implement and execute and presents effective results, not needing to use deep learning networks.

Table 3. Results generated by the proposed method and by the algorithm based on the Detectron 2 deep learning network together with fine-tuning techniques.

Algorithm	ACC	DSC	TPR	SPC
LSBRD-μ	**99.85 ± 0.07**	**93.35 ± 2.80**	**93.35 ± 4.23**	**99.94 ± 0.05**
Detectron 2 Han et al. (2020)	99.89 ± 0.05	94.81 ± 2.11	92.79 ± 3.87	99.97 ± 0.03
Detectron-$\boldsymbol{f\lambda}$ Han et al. (2020)	99.83 ± 0.06	91.37 ± 3.70	85.21 ± 6.29	99.99 ± 0.02
Detectron-$\boldsymbol{f\delta}$ Han et al. (2020)	99.88 ± 0.05	94.09 ± 2.40	90.89 ± 4.57	99.97 ± 0.03
Detectron-$\boldsymbol{f\mu}$ Han et al. (2020)	99.88 ± 0.05	94.04 ± 2.42	90.61 ± 4.54	99.98 ± 0.03

Table 4. Time of convergence of the evaluated methods.

Initialization	Algorithm	Time
Traditional Approach	**LSBRD-μ**	**1.140±0.040**
	Medeiros et al. Medeiros et al. (2020)	2.200±0.210
	Rebouças et al. Rebouças et al. (2017)	1.760±0.290
	Rouhi et al.Rouhi et al. (2015)	3.100±1.700
	Korbe et al. Körbes and Lotufo (2010)	4.800±0.620
	Dunn Dunn (1973)	8.690±3.160
Deep Learning based Approach	Detectron 2	0.095±0.006
	Detectron-$\boldsymbol{f\lambda}$	3.082±1.897
	Detectron-$\boldsymbol{f\delta}$	3.415±2.003
	Detectron-$\boldsymbol{f\mu}$	4.534±1.089

6. CONCLUSION

In this work, a new hemorrhagic stroke (HS) segmentation method in CT images of the skull bein proposed using an approach based on the junction of the μ law with the non-parametric Parzen Window estimation method, called LSBRD-μ. As method validation, the database described in 3.5 bein used, and the segmentation obtained was compared with traditional methods in the literature and with approaches that use deep learning.

The similarity indices show how close is the segmentation of the lesions marked by the specialist. In this sense, the method presented a degree of similarity superior to the other traditional algorithms, being the only one to exceed 92% for the MCC and DSC indices and with the lowest standard deviation, 2.68%, and 2.80%, respectively. In addition, it was the only one to surpass the 85% mark for the JSC metric. That shows how close the lesion obtained is to that produced by specialists.

The LSBRD-μ is effective in determining if the localized region is damaged. That can bein confirmed by the high value of ACC (99.85%). That indicates that the method can predict with almost 100% accuracy that the pixels obtained are, in fact, from the region of interest. In addition, the value obtained in the SPC metric (99.94%), which is the highest among all, indicates that the method is the best in detecting non-stroke regions.

Regarding the methods that use deep learning and need GPU, as they are computationally expensive for CPU processing, LSBRD-μ reached 93.35% in the SEN index, thus superior to all other methods.

Regarding the segmentation time, presented in Table 4, the LSBRD-μ showed an average time of approximately 1 second per image with a standard deviation of 0.04 seconds. Thus, the proposed method is the fastest among the traditional algorithms and is the second-fastest compared to the deep learning algorithms.

Therefore, based on the analyzes made above, it is concluded that the proposed algorithm is efficient in correctly segmenting the hemorrhagic stroke in brain CT images and with a low cost of processing time per image.

ACKNOWLEDGMENTS

This study was financed in part by the Coordenação de Aperfeiçoamento de Pessoal de Nível Superior-Brasil(CAPES) Finance Code 001". Also Pedro Pedrosa Rebouças Filho acknowledges the sponsorship from the Brazilian National Council for Research and Development (CNPq) via Grants Nos. 431709/2018-1 and 311973/2018-3.

REFERENCES

Benson, C., Lajish, V., and Rajamani, K. (2015). Brain tumor extraction from mri brain images using marker based watershed algorithm. In *2015 International Conference on Advances in Computing, Communications and Informatics (ICACCI)*, 318–323. IEEE.

Bishop, C.M. (2006). *Pattern Recognition and Machine Learning (Information Science and Statistics)*. Springer-Verlag New York, Inc., Secaucus, NJ, USA.

de Souza Rebouças, E., de Medeiros, F.N.S., Marques, R.C.P., Chagas, J.V.S., Guimarães, M.T., Santos, L.O., Medeiros, A.G., and Peixoto, S.A. (2021). Level set approach based on parzen window and floor of log for edge computing object segmentation in digital images. *Applied Soft Computing*, 105, 107273.

Dunn, J.C. (1973). A fuzzy relative of the isodata process and its use in detecting compact well-separated clusters.

Faruque, S. (2015). Pulse code modulation (pcm). In *Radio Frequency Source Coding Made Easy*, 65–90. Springer.

Han, T., Nunes, V.X., Souza, L.F.D.F., Marques, A.G., Silva, I.C.L., Junior, M.A.A.F., Sun, J., and Reboucas Filho, P.P. (2020). Internet of medical things—based on deep learning techniques for segmentation of lung and stroke regions in ct scans. *IEEE Access*, 8, 71117–71135.

Hossin, M. and Sulaiman, M. (2015). A review on evaluation metrics for data classification evaluations. *International Journal of Data Mining & Knowledge Management Process*, 5(2), 1.

Karthik, R. and Menaka, R. (2017). A multi-scale approach for detection of ischemic stroke from brain mr images using discrete curvelet transformation. *Measurement*, 100, 223–232.

Körbes, A. and Lotufo, R. (2010). Analise de algoritmos da transformada watershed. In *17th International Conference on Systems, Signals and Image Processing*.

Medeiros, A.G., Santos, L.d.O., Sarmento, R.M., de Souza Rebouças, E., and Rebouças Filho, P.P. (2020). New adaptive morphological geodesic active contour method for segmentation of hemorrhagic stroke in computed tomography image. In *Brazilian Conference on Intelligent Systems*, 604–618. Springer.

Oesch, L., Arnold, M., Bernasconi, C., Kaesmacher, J., Fischer, U., Mosimann, P.J., Jung, S., Meinel, T., Goeldlin, M., Heldner, M., et al. (2021). Impact of pre-stroke dependency on outcome after endovascular therapy in acute ischemic stroke. *Journal of neurology*, 268(2), 541–548.

Osher, S. and Sethian, J.A. (1988). Fronts propagating with curvature-dependent speed: algorithms based on hamilton-jacobi formulations. *Journal of computational physics*, 79(1), 12–49.

Rebouças, E.d.S., Braga, A.M., Sarmento, R.M., Marques, R.C., and Rebouças Filho, P.P. (2017). Level set based on brain radiological densities for stroke segmentation in ct images. In *2017 IEEE 30th International Symposium on Computer-Based Medical Systems (CBMS)*, 391–396.

Reboucas, E.d.S., Marques, R.C., Braga, A.M., Oliveira, S.A., de Albuquerque, V.H.C., and Reboucas Filho, P.P. (2019). New level set approach based on parzen estimation for stroke segmentation in skull ct images. *Soft Computing*, 23(19), 9265–9286.

Reboucas, E.S., Braga, A.M., Marques, R.C., and Reboucas Filho, P.P. (2016). A new approach to calculate the nodule density of ductile cast iron graphite using a level set. *Measurement*, 89, 316–321.

Rebouças, E., Braga, A., Sarmento, R., Marques, R., and Filho, P.P. (2017). Level set based on brain radiological densities for stroke segmentation in ct images. doi: 10.1109/CBMS.2017.172.

Ribeiro, M.A.B. (2017). Estudo de um modelo de conversor a/d com níveis de quantização configuráveis.

Rouhi, R., Jafari, M., Kasaei, S., and Keshavarzian, P. (2015). Benign and malignant breast tumors classification based on region growing and cnn segmentation. *Expert Systems with Applications*, 42(3), 990–1002.

Sethian, J.A. (1999a). *Level Set Methods and Fast Merging Methods: Evolving Interfaces in Computational Geometry, Fluid Mechanics, Comput. Vision and Materials Science*. Cambridge University Press, Cambridge, 1 edition.

Sethian, J.A. (1999b). *Level set methods and fast marching methods: evolving interfaces in computational geometry, fluid mechanics, computer vision, and materials science*, volume 3. Cambridge university press.

Sivakumar, P. and Ganeshkumar, P. (2017). An efficient automated methodology for detecting and segmenting the ischemic stroke in brain mri images. *International Journal of Imaging Systems and Technology*, 27(3), 265–272.

Theodoridis, S. and Koutroumbas, K. (2009). Classifiers based on bayes decision theory. In S. Theodoridis and K. Koutroumbas (eds.), *Pattern Recognition*, 13 – 89. Academic Press, Boston, 4 edition.

Virani, S.S., Alonso, A., Benjamin, E., Bittencourt, M., Callaway, C., Carson, A., Chamberlain, A., Chang, A., Cheng, S., Delling, F., et al. (2020). American heart association council on epidemiology and prevention statistics committee and stroke statistics subcommittee. *Heart disease and stroke statistics-2020 update: a report from the American Heart Association. Circulation*, 141(9), e139–e596.

Yahiaoui, A.F.Z. and Bessaid, A. (2016). Segmentation of ischemic stroke area from ct brain images. In *Signal, Image, Video and Communications (ISIVC), International Symposium on*, 13–17. IEEE.

Yeung, D. and Chow, C. (2002). Parzen-window network intrusion detectors. In *16th International Conference on Pattern Recognition*, 385–388. Int Assoc Pattern Recognit, Quebec City, Canada.

Zhang, R., Zhao, L., Lou, W., Abrigo, J.M., Mok, V.C., Chu, W.C., Wang, D., and Shi, L. (2018). Automatic segmentation of acute ischemic stroke from dwi using 3-d fully convolutional densenets. *IEEE transactions on medical imaging*, 37(9), 2149–2160.